Acta Pharmaceutica Sinica B 2025;15(6):3291−3304

Chinese Pharmaceutical Association
Institute of Materia Medica, Chinese Academy of Medical Sciences

Acta Pharmaceutica Sinica B

www.elsevier.com/locate/apsb
www.sciencedirect.com

ORIGINAL ARTICLE

Tranexamic acid-fatty alcohol polyoxyethylene ether conjugation/PVA foam for venous sclerotherapy *via* vascular damage and inhibiting plasmin system

Jizhuang Ma[a,†], Keda Zhang[b,†], Wenhan Li[c], Yu Ding[a], Yongfeng Chen[a], Xiaoyu Huang[a], Tong Yu[a], Di Song[a], Haoran Niu[a], Huichao Xie[b], Tianzhi Yang[d], Xiaoyun Zhao[e,*], Xinggang Yang[a,*], Pingtian Ding[b,a,*]

[a]*School of Pharmacy, Shenyang Pharmaceutical University, Shenyang 110016, China*
[b]*College of Pharmacy, Shenzhen Technology University, Shenzhen 518118, China*
[c]*Ultrasound Department, Shengjing Hospital, China Medical University, Shenyang 110016, China*
[d]*Department of Basic Pharmaceutical Sciences, School of Pharmacy, Husson University, Bangor, ME 04401, USA*
[e]*School of Life Science and Biopharmaceutics, Shenyang Pharmaceutical University, Shenyang 110016, China*

Received 15 September 2024; received in revised form 10 December 2024; accepted 19 January 2025

KEY WORDS

Tranexamic acid;
Fatty alcohol polyoxyethylene ether;
Foam preparation;
Plasmin system;
Matrix metalloproteinases;
Venous malformations;
Sclerotherapy;
Fibrosis

Abstract Venous system diseases mainly include varicose veins and venous malformations of lower limbs and the genital system. Most of them are chronic diseases that cause serious clinical symptoms to patients and affect their health and quality of life. Sclerotherapy has become the first-line therapy for venous system diseases. However, there are problems such as incomplete fibrosis and vascular recanalization after sclerotherapy, and improper operation will cause serious adverse consequences. Therefore, exploring a safe and effective sclerotherapy strategy is essential for developing clinically successful sclerotherapy. To solve the above problems, we proposed a new sclerotherapy strategy with a dual mechanism of "vascular damage and plasmin (PLA) system inhibition." We intended to construct a novel cationic surfactant (AEO_x-TA) by reacting tranexamic acid (TA), a parent structure, with fatty alcohol polyoxyethylene ether (AEO_x) by ester bonds. AEO_x-TA could damage vascular endothelium and initiate a coagulation cascade effect to induce thrombus. Furthermore, AEO_x-TA could be degraded by esterase

*Corresponding authors.
E-mail addresses: zhaoxiaoyun@syphu.edu.cn (Xiaoyun Zhao), yangxg123@163.com (Xinggang Yang), dingpingtian@sztu.edu.cn (Pingtian Ding).
†These authors made equal contributions to this work.

Peer review under the responsibility of Chinese Pharmaceutical Association and Institute of Materia Medica, Chinese Academy of Medical Sciences.

https://doi.org/10.1016/j.apsb.2025.03.032

and release the parent drug, TA, which could inhibit the PLA system to inhibit the degradation of thrombus and extracellular matrix and promote the process of vascular fibrosis. In addition, such surfactant-based sclerosants have foam-forming properties, and they can be blended with polyvinyl alcohol (PVA) to prepare a highly stable foam formulation (AEO_x-TA/P), which can achieve a precise drug delivery and prolonged drug retention time, thereby improving drug efficacy and reducing the risk of ectopic embolism. Overall, the novel cationic surfactant AEO_x-TA provides a new avenue to resolve the bottleneck: surfactant sclerosants' efficiency is relatively low in the current sclerotherapy.

1. Introduction

Venous system diseases mainly include varicose veins and venous malformations of lower limbs and the genital system[1]. Venous diseases are primarily chronic diseases and impose severe clinical symptoms on patients, therefore severely affecting their health and quality of life[2,3]. Currently, sclerotherapy has become the first line of treatment for venous diseases[4]. Vein sclerosing may be achieved by injecting sclerosants directly into the blood vessels and through chemical stimulation. This causes local endothelial cell damage, which leads to endothelial stripping, collagen fiber shrinkage, thrombosis, blood vessel occlusion, and eventually damage to the fibrous cord[5]. Common sclerotherapy drugs include anhydrous ethanol, sodium morrhuate (SM), pingyangmycin, and bleomycin[6-10]. However, these agents often suffer from poor retention at the target site when administered in a liquid form. Moreover, these sclerosing agents may dilute in the bloodstream and spread to invade the capillary network, thereby causing various serious complications[11].

Polidocanol (POL) and sodium tetradecyl sulfate (STS) in the form of foam as a drug delivery system have been reported to significantly improve the vascular retention of sclerosants and reduce the side effects of drugs[12-15]. However, STS and POL, which are anionic and non-ionic surfactants, respectively, have shown low injury intensity to blood vessels and poor foam stability[16-18]. Despite these limitations, significant strides have been made in drug delivery and endothelium targeting within sclerotherapy [19-23], including the development of nanomedicines[24,25]. For example, Jiang and coworkers[25] have designed light-activated gold nanorods to treat venous malformation effectively. Some other studies have focused on increasing foam stability and improving the vascular damage effect of POL[14,26]. For example, Sun and colleagues[26] developed a bleomycin POL foam for venous malformation sclerotherapy. However, combining these sclerosants may increase the risk of systemic toxicity, highlighting the need for safer and more effective sclerotherapy strategies.

Fatty alcohol polyoxyethylene ether (AEO_x) is an amphiphilic material with an alkyl carbon chain and ethylene oxide chain connected by an ether bond, serving as a typical nonionic surfactant[27]. Adjusting the length of the alkyl carbon chain and the number of ethylene oxide units (denoted as x) could alter the material's hydrophilic-lipophilic balance (HLB)[28]. By mixing with 1% polyvinyl alcohol (PVA), AEOx can generate stable foam through mechanical agitation, thus improving the retention of the drug at the target site[29]. It is worth mentioning that POL is one of the AEO_x compounds, demonstrating the human safety of these materials. Current sclerotherapy strategies predominantly target damaging vascular endothelial cells, neglecting the processes of vascular fibrosis, leading to incomplete fibrosis and potential vascular recanalization after treatment. In recent years, in-depth studies on the mechanism of plasmin (PLA) have revealed that PLA not only dissolves thrombi but also promotes apoptosis of myofibroblasts, activates matrix metalloproteinases (MMPs) to degrade collagen produced by tissues, affects the expression of signaling factors that promote fibrosis, and ultimately inhibits the fibrosis process in damaged tissues[30-36]. Tranexamic acid (TA), also known as thrombin acid, is a synthetic lysine analog. Its affinity for PLA is stronger than that of the lysine residues in fibrin, which helps stabilize the fibrin matrix by inhibiting its dissolution[37-39]. The structure of TA contains amino and carboxyl groups at both ends, so TA does not have surface activity, causing any damage to cells[39]. Our previous study found that the carboxyl group of TA connecting the hydrophobic or amphiphilic long chain fragments with ester bonds could form a type of cationic surfactant sclerosant[40]. In addition, the ester bonds of sclerosants can be degraded by esterase to release TA, thereby losing the cationic surfactant properties of sclerosants and greatly improving safety.

This study aimed to develop a more effective cationic surfactant sclerosant, AEOx-TA, to enhance sclerotherapy through a dual mechanism: damaging blood vessels and intervening in the PLA system. The carboxyl-terminal of TA was connected to the AEO_x by ester bonds to build a new cationic surfactant type sclerosant (AEO_x-TA). The vascular sclerosing mechanism of AEO_x-TA is shown in Scheme 1. After mixing with 1% PVA, AEO_x-TA was formulated into a foam preparation (AEO_x-TA/P) and injected into target blood vessels. The foam can displace part of the blood and enhance the contact area and duration between the drug and blood vessel walls[41]. The sclerosants then damage the affected blood vessels by compromising the integrity of the vascular endothelial cell membrane. The damage to endothelial cells within blood vessels can trigger the formation of thrombus and contribute to the progression of vascular fibrosis. Simultaneously, the fibrinolytic system is activated, and AEO_x-TA can be degraded by esterases, releasing TA, which inhibits the activity of PLA. This inhibition prevents thrombus degradation, thus reducing the risk of embolism and vascular recanalization. Furthermore, inhibiting the PLA system also suppresses the activation of MMPs, facilitating the accumulation of matrix proteins at the vascular site. This promotes fibroblast proliferation and advances the process of vascular fibrosis. Thus, this innovative sclerotherapy approach based on AEO_x-TA/P offers a promising new avenue for strategic research in the field.

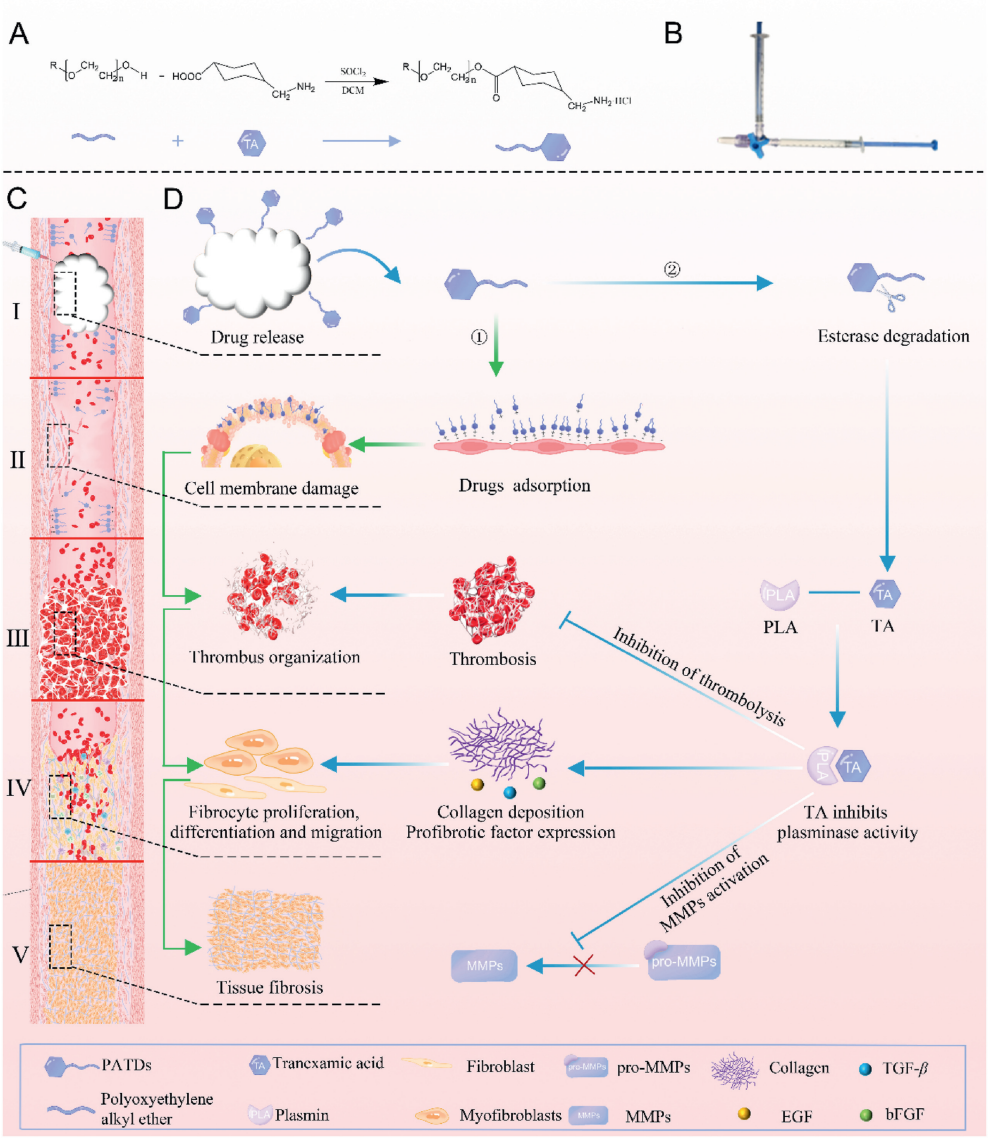

Scheme 1 (A) AEO_x-TA synthesis route. (B) The syringe mixing process of AEO_x-TA/P foam preparation is done using the Tessari method. (C) Vascular sclerosing process illustration of AEO_x-TA foam sclerotherapy (I injection of AEO_x-TA/P foam preparation, II vascular damage, III thrombosis, IV formation of tissue fibrosis microenvironment, V vascular fibrosis). (D) "vascular damage-fibrinolytic system inhibition" dual mechanism of vascular sclerosis.

2. Materials and methods

2.1. *Synthesis of AEO_x-TA and characterization*

TA (6 mmol) was added into a 500 mL three-neck flask, and dichloromethane (200 mL) was added as a solvent. The reaction system was cooled under an ice bath for 30 min. Sulfoxide chloride (7.2 mmol) was slowly added under an ice bath, and the reaction was continued for 12 h at 25 °C. Next, AEO_3, AEO_5, AEO_7, AEO_9, AEO_{12}, and AEO_{15} (8.4 mmol) were slowly added, respectively, and continued to react at room temperature for 24 h. Subsequently, the dichloromethane was removed under reduced pressure, and the product was collected. The crude product was finally purified by automatic silica column chromatography (Santai technologies, SepaBean, Changzhou, China) eluting with dichloromethane/methanol (90:10−20:80, *v*/*v*), filtered under pressure, dried overnight under vacuum, and the purified product was obtained. AEO_x-TA was then characterized by Fourier transform infrared (FT-IR) and nuclear magnetic resonance (NMR). FT-IR spectra were recorded in the range between 4000 and 400 cm^{-1} on an FT-IR spectrophotometer (Thermo Nicolet iS50, Madison, Wisconsin). The ^1H NMR spectra of AEO_x-TA were measured using an NMR spectrometer (Bruker AV-400, Karlsruhe Germany) with D_2O as a solvent.

2.2. *Foam preparation and characterization*

AEO_x-TA/P foams were prepared according to the Tessari method, as previously reported[42]. First, we evaluated the effect of air volume on the stability of the AEO_x-TA foam preparations. Briefly, AEO_x-TA (0.1 mL, 3%) was put in one syringe, and X mL of air (gas−liquid ratio: X: 1) in the other syringe. Thirty pumping

cycles were performed to produce foams. After the foam preparation was complete, push all the foam into a 1 mL syringe and record the time when the foam changed into half of the original volume of solution. This was denoted as the foam half-time (FHT), which was used to represent the stability of foam preparations. Furthermore, we evaluated the influences of pumping cycle numbers and the concentration of AEO_x-TA on the stability of the AEO_x-TA foams. Similarly, 0.1 mL of 3% AEO_x-TA was put in one syringe, 0.4 mL air was put in the other syringe, and X numbers of pumping cycles were performed to produce foams to investigate the influence of pumping cycles on foam stability. Next, 0.1 mL AEO_x-TA with different concentrations (1%, 2%, 3%) was put in one syringe, and the 0.4 mL air was put in the other syringe. Thirty pumping cycles were performed to produce foams and investigate the influence of different AEO_x-TA concentrations on foam stability. Besides, 0.1 mL of 3% AEO_x-TA containing 0.5, 1%, and 2% PVA was put in one syringe and the 0.4 mL air was put in the other syringe, and 30 pumping cycles were performed to produce foams to investigate the influence of PVA concentrations on foam stability. Each group of tests was repeated ten times. What's more, the foam preparations under different conditions were observed and photographed under a microscope (Leica S9, Wetzlar, Germany), and the foam diameter distribution was recorded. Finally, the foam formulation is injected into the Vevo imaging tube, and then the ultrasound gel is applied between the imaging tube and the ultrasound probe (FUJIFILM VisualSonics, Vevo LAZR-X, Toronto, Canada). Utilize an ultrasound probe with a central frequency of 40 MHz for B-Mode imaging of the foam.

2.3. Cytotoxicity test

HUVEC-TIE2-L914F cells (4×10^3 cells per well) were grown overnight in 96-well plates and incubated with different concentrations of AEO_x-TA for another 12 h. After the cells were changed with new culture media, 10 μL of CCK-8 solution was added to each well and incubated for 2 h. The absorbance of the mixture in each well was then measured at 450 nm wavelength on a microplate reader (BioTek, Synergy H1, Vermont, US). Subsequently, cell apoptosis was determined according to the instructions of the Cell Apoptosis Kit. Briefly, HUVEC-TIE2-L914F cells (1×10^6 cells per well) were grown overnight in 6-well plates and incubated with AEO_x-TA (100 μmol/L) for another 12 h. Cells were collected and resuspended by phosphate buffer solution (PBS), stained with Annexin V-FITC and PI at room temperature for 15 min, and the cell apoptosis was determined within 1 h by a flow cytometer (Beckman Coulter, CytoFLEX, California, US).

2.4. Cell membrane and membrane protein destruction

HUVEC-TIE2-L914F cells (1×10^3 cells per well) were inoculated into 96-well plates and incubated overnight and incubated with AEO_x-TA (100 μmol/L) for another 12 h. The group with no cells was the negative group, and the group without AEO_x-TA was the positive group. The positive group was treated with lactate dehydrogenase release reagent, and the supernatant was collected. The other groups were centrifuged with a porous plate centrifuge (Cence, TG16-W, Hunan, China) at 400 g for 5 min, then 120 μL of supernatant was taken from each well and added to another 96-well plate. Then, the absorbance was measured at 490 nm by a microplate reader (BioTek).

In order to investigate the elution effect of AEO_x-TA on membrane proteins, HUVEC-TIE2-L914F cells (1×10^6 cells per well) were inoculated in 6-well plates and cultured overnight. The cells were treated with different AEO_x-TA ($x = 3$, 5, 7, 9, 12, or 15; 100 μmol/L of TA) for 12 h. Next, the cells were washed with PBS three times and fixed with 4% paraformaldehyde. Subsequently, goat serum was used to block the cell surface, and a FITC-labeled Cadherin protein antibody was added. Finally, the stained cell membrane protein was observed by a laser confocal microscope (Leica, STELLARIS 5, Wetzlar, Germany).

2.5. Degradability of AEO_x-TA and in vitro PLA-MMPs system inhibition

To investigate the degradability of the ester bond of AEO_x-TA, the AEO_x-TA were incubated with 10% serum in a water bath at 37 °C. Subsequently, four times the volume of ice methanol was added to stop the reaction at the scheduled time, and the supernatant was obtained by centrifugation (Cence, TGL-16, Hunan, China) at $15{,}000 \times g$. The content of TA was determined by liquid chromatography-mass spectrometry (HPLC-MS; Thermo Scientific, Orbitrap 120, Massachusetts, US). To investigate the inhibition of TA, a degradation product from AEO_x-TA, on PLA and MMPs, the products from AEO_x-TA degraded by 2.5% esterase for 10 min were mixed with PLA solution and incubated for another 12 h. Next, part of the above solution was incubated with proMMP9 solution. Finally, the synthetic luminescent substrate method was used to determine the activity of PLA[43,] and the enzyme activity of MMP9 was determined using a gelatinase assay[32].

2.6. Evaluation of embolus in mouse tail vein

Kunming mice were divided into the saline group, POL/P foam preparation group, and AEO_x-TA/P foam preparation group ($n = 6$). The vein of mice was photographed under irradiation of 0.5 W light emitting diode (LED) yellow light (Globalebio, GEGD-Q9G, Beijing, China) every 24 h after the administration of treatments (with concentrations of TA at 30 mmol/L, 0.1 mL). Afterward, blood samples were collected from mouse orbits, and cells were separated using a Percoll density gradient centrifugation method, as previously described, after 24 h of administration. The upper layer cells were collected, and circulating endothelial cells (CECs) were counted under a microscope (Leica DMi1, Wetzlar, Germany). All experimental procedures were executed according to the protocols approved by Shenyang Pharmaceutical University's Animal Care and Use Committee.

2.7. Evaluation of embolus in rabbit ear marginal vein

Ear vein of healthy New Zealand rabbits was selected as the therapeutic vessel model, and the experimental animals were divided into the TA group, AEO_{15}/P foam group, AEO_{15} and TA physical mixture (AEO_{15}+TA/P) foam group, and AEO_{15}-TA/P foam group. The blood vessels were photographed by the camera (Fujifilm, X−S20, Tokyo, Japan) and observed every day after the administration of treatments (with concentrations of TA at 30 mmol/L, 0.2 mL). The embolization length of the treatment vessels and the time for the emboli to disappear in the treatment vessels were measured to evaluate the sclerosing effect. All experimental procedures were executed according to the protocols

approved by Shenyang Pharmaceutical University's Animal Care and Use Committee.

3. Results and discussions

3.1. Synthesis and characterization of AEO_x-TA

In this study, a PLA inhibitor, TA, was connected with AEO_x by ester bonds to build a new cationic surfactant sclerosant, AEO_x-TA. The sclerosant solution was mixed with air to prepare a foam and then injected into blood vessels. The AEO_x-TA, as a cationic surfactant, can destroy the cell membrane, causing blood vessel damage and thereby stimulating thrombus generation. Subsequently, the degradability of ester bonds in AEO_x-TA by esterase can release TA to inhibit the PLA system and promote the process of vascular fibrosis. AEO_x-TA was constructed using an acyl chloride esterification reaction to connect TA with six kinds of AEO_x. AEO_x comprised 12-carbon straight-chain alkane as hydrophobic fragments and 3, 5, 7, 9, 12, or 15 ethylene oxide units as hydrophilic fragments through ether bonds. The hydrophilicity was enhanced with the increase in the number of ethylene oxide units.

FT-IR was used to characterize AEO_x-TA. Fig. 1A represents the infrared absorption spectrum of AEOx, and Fig. 1B represents the infrared absorption spectrum of AEO_x-TA. Compared with the infrared absorption spectrum of AEO_x, the AEO_x-TA showed a stronger absorption peak at the wavelength of 1750 cm^{-1}, which belonged to the ester bond absorption peak, indicating the successful synthesis of AEO_x-TA. Furthermore, AEO_x-TA was characterized by a ^1H NMR spectrum, and the results are shown in Supporting Information Fig. S1. The ^1H NMR spectrum showed characteristic peaks of AEO_x-TA, indicating that AEO_x-TA was successfully synthesized. In addition, the yields of AEO_3-TA, AEO_5-TA, AEO_7-TA, AEO_9-TA, AEO_{12}-TA and AEO_{15}-TA were determined to be 98.83%, 97.62%, 96.54%, 96.21%, 96.11%, and 96.05%, respectively.

AEO_x-TA is a type of surfactant sclerosant, and the surfactant parameters of AEO_x-TA were measured. First, the HLB value of AEO_x-TA was measured by a classical emulsification method, and the results are shown in Fig. 1C. The HLB values of AEO_3-TA, AEO_5-TA, AEO_7-TA, AEO_9-TA, AEO_{12}-TA, and AEO_{15}-TA were 5.5, 10, 11.2, 13, 14.5, and 16, respectively, indicating that the HLB value increased gradually with the growth of the hydrophilic chain. Next, the surface tension was measured, and the results are shown in Fig. 1D. The surface tensions of AEO_3-TA, AEO_5-TA, AEO_7-TA, AEO_9-TA, AEO_{12}-TA, and AEO_{15}-TA in aqueous solution were 60.2, 56.3, 45.2, 42.3, 36.5, 32.8 mN/m, indicating that with the increasing length of the hydrophilic chain, the ability of surfactant to reduce the surface tension of aqueous solution was enhanced gradually. The surfactant parameters of AEO_x-TA determine the stability of foam preparation and the sclerosing effect in vascular sclerotherapy.

The result of the electric potential of AEOx-TA is shown in Fig. 1E. The electric potential of AEO_x-TA was about 15 mV, indicating that AEO_x-TA was a cationic surfactant. The interaction between sclerosant and phospholipid membrane was measured using Langmuir film balance by mixing monolayer AEO_x-TA with DPPC; the result was shown in Fig. 1F and H. The excess molecular area and excess Gibbs energy of AEO_x-TA were decreased with the increase of the hydrophilic chain, indicating that the interaction between AEO_x-TA and DPPC was enhanced with the increase of the hydrophilic chain. It can be inferred from the results that an increase in the length of the hydrophilic chain could contribute to the amino group of AEOx-TA touching with DPPC.

3.2. Foam preparation and characterization

Surfactant sclerosants have the advantage of foaming properties. The foam preparation can replace part of the blood in the blood vessel and enhance the contact between the drug and the blood vessel. Therefore, we investigated the optimal formulation of AEO_x-TA/P foam preparations based on the foam stability. We considered three key factors, including gas−liquid ratio, number of pumping cycles, and drug concentration, to assess the foam stability. According to previous reports[14], the general range of gas−liquid ratio was set as 1:3−1:5, the number of pumping cycles was not less than 20 times, and the drug concentration was in the range of 1%−3%. Firstly, we investigated the influence of gas−liquid ratios on the stability of foam formation. The Tessari method was used to prepare the foams. AEO_x-TA solution (0.1 mL with 2% of AEOx-TA) was put into one syringe, and 0.3, 0.4, and 0.5 mL air was put in the other syringe, respectively. Thirty pumping cycles were performed to produce foams. The time when the foam changed into half of the original volume of solution was recorded. According to the results of Supporting Information Fig. S2, AEO_3-TA could not be used to prepare foam preparations due to its strong hydrophobicity and insolubility in water. For AEO_5-TA, it was slightly soluble in water, and the foam formed was relatively stable when the gas−liquid ratio was 3:1. For AEO_7-TA, AEO_9-TA, AEO_{12}-TA, and AEO_{15}-TA, these sclerosants could form stable foams when the gas−liquid ratio was 4:1. These results indicated that when the foaming properties of surfactants were weak, more surfactant solution and less gas were needed. In contrast, the stronger the foaming properties of surfactants, the more gas could be converted into foams, thus reducing the dosage of sclerosant. Therefore, it could reduce the toxic side effects caused by excessive drugs in sclerotherapy when more gas was used to prepare foam preparation.

We investigated the influence of push and pull times and drug concentration on foam stability. According to the results, under the optimal gas−liquid ratio of each group, the stability of foam gradually increased with the increase of push and pull times and drug concentration. When the push and pull times reached 30 times, and drug concentration reached 2%, the stability of foam tended to be stable. What's more, the FHT of AEO_x-TA foam under optimal conditions was statistically analyzed, and the results are shown in Fig. 1I. The average FHTs of AEO_3-TA, AEO_5-TA, AEO_7-TA, AEO_9-TA, AEO_{12}-TA, and AEO_{15}-TA were 11, 45, 138, 142, 148, and 155 s, respectively. The results indicated that AEO_3-TA and AEO_5-TA foam preparations were unstable, while AEO_7-TA and AEO_9-TA could form relatively stable foam bubbles, and AEO_{12}-TA and AEO_{15}-TA could form the most stable bubbles. It can be inferred from the results that the HLB value and surface tension of the surfactant had a great influence on the stability of the foam, and the stability of the foam was gradually enhanced with the growth of the hydrophilic chain of AEO_x-TA. In order to enhance the stability of the foam further, we have chosen a high molecular weight polymer material, PVA, which is highly biocompatible, to increase the viscosity of the foam. The results demonstrate that the addition of 1% PVA, AEO_3-TA/P, AEO_5-TA/P, AEO_7-TA/P, AEO_9-TA/P, AEO_{12}-TA/P, and AEO_{15}-TA/P has increased the half-life of the foam to 15, 62, 263, 286, 301, and 310 s respectively. The viscosity of the foam was

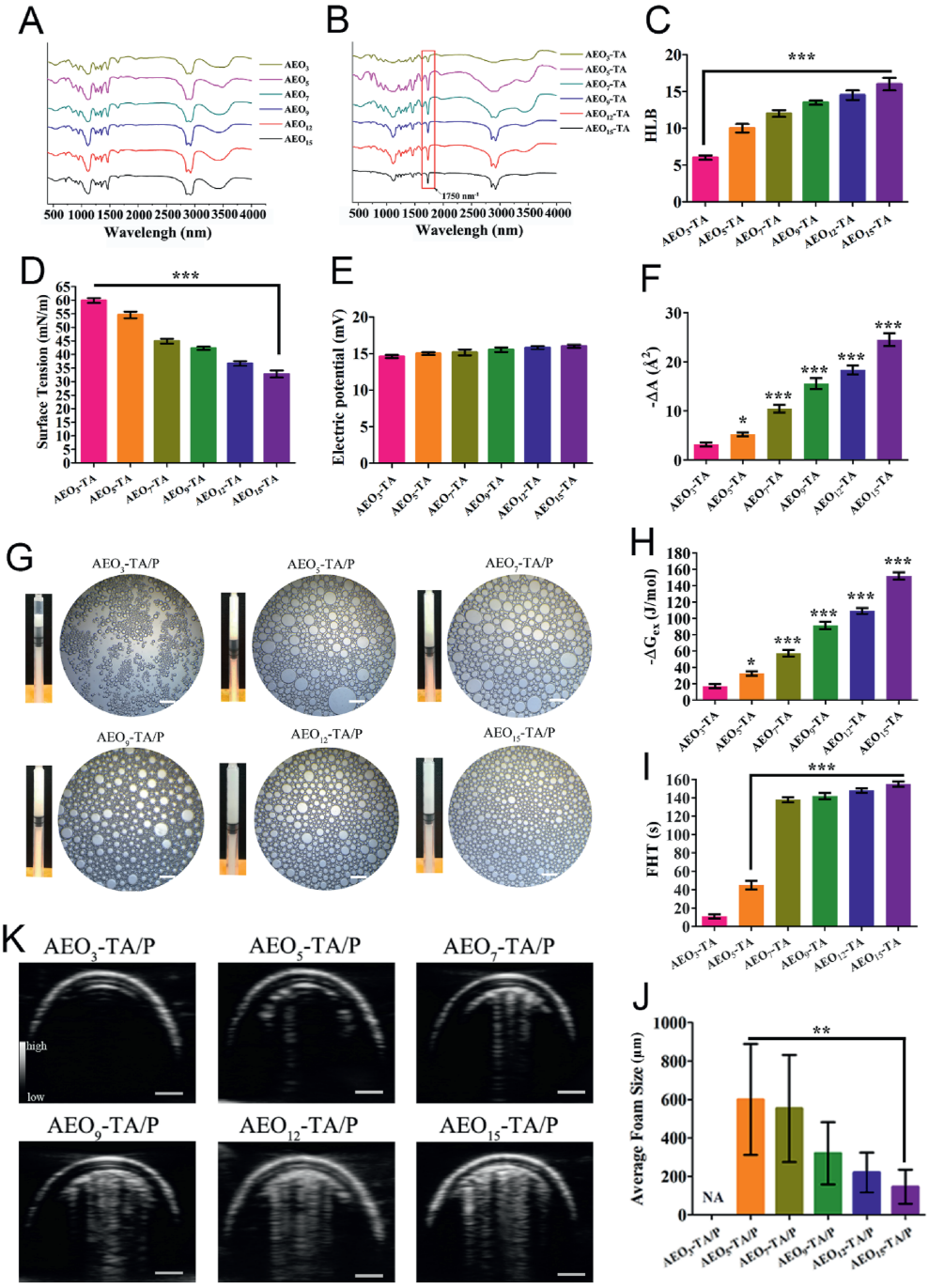

Figure 1 (A) Infrared absorption spectra of AEO_x. (B) Infrared absorption spectra of AEO_x-TA. (C) HLB value of AEO_x-TA. (D) Surface tension of AEO_x-TA. (E) The electric potential of AEO_x-TA. (F) Excess intermolecular distance of mixture of DPPC and AEO_x-TA. (G) AEO_x-TA/P foam preparation viewed under a microscope, scale bar = 500 μm. (H) Excess Gibbs energy of the mixture of DPPC and AEO_x-TA. (I) FHT of AEO_x-TA foam preparation. (J) Average foam size of AEO_x-TA/P (NA = not available). (K) 2D B-Mode ultrasound imaging of AEO_x-TA/P foam preparation (scale bar = 0.5 mm). Data are presented as mean ± SD (n = 6), $^*P < 0.05$, $^{**}P < 0.01$, $^{***}P < 0.001$; ns, not significant.

measured using a rheometer, and the result is shown in Supporting Information Fig. S3. The viscosity of the foam without the presence of PVA was about 700 mPa s. However, after the addition of PVA, the viscosity of the foam increased to 1500 mPa·s. This indicates that the addition of 1% PVA has improved the foam stability through the enhancement of its viscosity.

The foams prepared under different preparation conditions were observed under a microscope, and the average particle sizes of the foams were statistically analyzed. The results are shown in Fig. 1G and J. AEO_3-TA/P could not form foam, while AEO_5-TA/P foam displayed many large bubbles due to its instability. The foams prepared by AEO_7-TA/P and AEO_9-TA/P were closely

arranged, but the foam sizes were not uniform, while the foams prepared by AEO_{12}-TA/P and AEO_{15}-TA/P were tightly arranged and the foam sizes were uniform. The uniformity of the foam particle sizes greatly influences its stability. When the size of the foam is not uniform, the small bubble will convert to a large bubble so that the bubble will burst faster. When the foam size is small and uniform, the specific surface area of the foam is larger, which is more suitable for vascular sclerotherapy. What's more, the foam was observed under Doppler ultrasound, and the result is shown in Fig. 1K. The AEO_3-TA/P and AEO_5-TA/P groups could not observe obvious signals due to the unstable foam. However, the AEO_7-TA/P, AEO_9-TA/P, AEO_{12}-TA/P, and AEO_{15}-TA/P could observe obvious signals under Doppler ultrasound, which is beneficial to observe the distribution of sclerosant foam in blood vessels under ultrasonography.

3.3. *Cytotoxicity of AEO_x-TA*

HUVEC-TIE2-L914F cell is a cell model of venous malformation approved by the FDA. We used a CCK-8 assay to investigate the cytotoxicity of AEO_x-TA to HUVEC-TIE2-L914F cells. As shown in Fig. 2A, with the increase in drug concentration, the

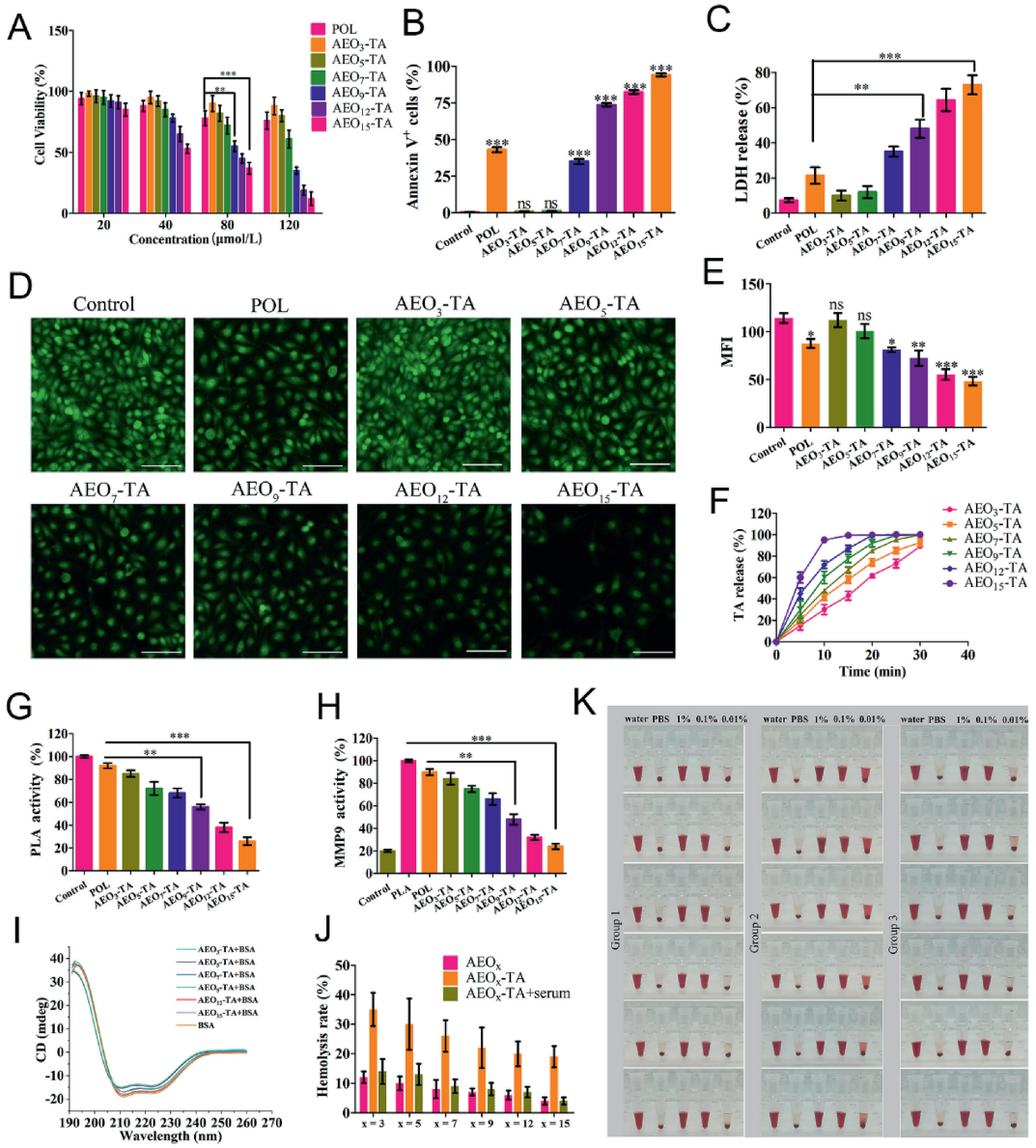

Figure 2 (A) *In vitro* cytotoxicity of POL and AEO_x-TA against HUVEC-TIE2-L914F cells for 12 h. (B) Cell apoptosis was detected in HUVEC-TIE2-L914F cells by flow cytometry. (C) LDH release of HUVEC-TIE2-L914F cells treated with POL and AEO_x-TA. (D) and (E) Immunofluorescence staining images and mean fluorescent intensity (MFI) of cadherin on HUVEC-TIE2-L914F cells, scale bar = 200 μm. (F) TA release rate of AEO_x-TA in 10% serum solution. (G) Inhibitory effects of the degradation product of AEO_x-TA on PLA. (H) MMP9 inhibition by the degradation product of AEO_x-TA. (I) CD spectra for BSA protein (0.1 mg/mL) incubated with different AEO_x-TA. (J) A hemolysis assay of 0.01% AEO_x, AEO_x-TA, and AEO_x-TA treated with 10% serum for 15 min. (K) Hemolysis assay of 1%, 0.1%, and 0.01% AEO_x (Group 1), AEO_x-TA (Group 2), and AEO_x-TA treated with 10% serum for 15 min (Group 3), from top to bottom, x = 3, 5, 7, 9, 12, and 15. Data are presented as mean ± SD (n = 6), *P < 0.05, **P < 0.01, ***P < 0.001; ns, not significant.

cytotoxicity of AEO_x-TA on HUVEC-TIE2-L914F cells gradually increased. In addition, with the increase of the hydrophilic fragment of AEO_x-TA, the cell viability decreased gradually, indicating that the cytotoxicity of surfactants increased significantly with the increase of hydrophilicity of AEO_x-TA. In addition, AEO_9 and POL have similar structures. Compared with the POL group, the cell viability of HUVEC-TIE2-L914F in the AEO_9-TA group was significantly reduced. The above results indicated that the cytotoxicity of AEO_x-TA, a cationic surfactant, was higher than that of POL, a non-ionic surfactant. This was because cationic surfactants could be adsorbed on the negatively charged cell membrane surface by electrostatic attraction. The morphology of HUVEC-TIE2-L914F cells treated with different sclerosants was observed under the microscope, and the results are shown in Supporting Information Fig. S4. After the AEO_x-TA treatment, cells displayed certain morphological changes. Moreover, most of the cells were detached from the plates. With the increase of the length of the hydrophilic chain of AEO_x-TA, more cells were detached from the plates, indicating that surfactant sclerosant could not only damage the cell membrane but also cause cell shedding.

3.4. Investigation of the cytotoxic mechanism of AEO_x-TA

We investigated the mechanism of HUVEC-TIE2-L914F cell damage caused by AEO_x-TA. Firstly, flow cytometry was used to analyze the apoptosis of HUVEC-TIE2-L914F cells induced by AEO_x-TA. As shown in Fig. 2B, the apoptosis of HUVEC-TIE2-L914F cells induced by sclerosant gradually increased with the increase of AEO_x-TA hydrophilic chain length. It can be seen from the results that the apoptosis caused by AEO_9-TA was significantly higher than that caused by POL, which indicated that the cationic surfactant had higher cytotoxicity. Moreover, the lactate dehydrogenase (LDH) experiment was used to investigate the damaging effect of AEO_x-TA on cell membranes. The damage to the cell membrane structure caused by apoptosis or necrosis led to the release of LDH in the cytoplasm into the culture medium. With this property, the damaging effect of AEO_x-TA on the cell membrane was investigated. As shown in Fig. 2C, the amount of LDH released from cells gradually increased with the increase of hydrophilicity of AEO_x-TA, which was similar to the result of CCK-8 cytotoxicity, indicating that part of the damage of AEO_x-TA to cells came from the damage to the cell membrane.

The immunofluorescence experiment was used to investigate the mechanism of cell shedding by AEO_x-TA. The results are shown in Fig. 2D and E and the green fluorescence represents cadherin. The green fluorescence intensity was still strong after AEO_3-TA and AEO_5-TA treatment, indicating that cadherin on the cell membrane did not elute significantly. After AEO_7-TA and AEO_9-TA treatments, the green fluorescence intensity was relatively weakened, indicating that most of the cadherin eluted from the cell membrane. After AEO_{12}-TA and AEO_{15}-TA treatment, the green fluorescence intensity was very weak, indicating that there was much cadherin was eluted from the cell membrane. These results suggested that the mechanism by which AEO_x-TA damaged cells was involved with the elution of proteins on the surface of the cell membrane, resulting in cell detachment. Based on the above results, it could be inferred that the mechanism of AEO_x-TA injury to vascular endothelial cells was that the amino group of the AEO_x-TA was adsorbed on the negatively charged cell membrane by electrostatic attraction, and then the hydrophobic part of AEO_x-TA was inserted into the phospholipid bilayer. Subsequently, the hydrophilic fragment of AEO_x-TA could drag the phospholipid bilayer into the aqueous phase, resulting in cell membrane damage. In addition, the amino group of the AEO_x-TA could also combine with amino acid residues such as aspartic acid and glutamic acid in the cell membrane proteins, resulting in the denaturing of the cell membrane proteins.

3.5. Degradability of AEO_x-TA and inhibition of PLA-MMPs system in vitro

Another feature of AEO_x-TA sclerotherapy is the release of TA to inhibit the PLA system. Firstly, the release rate of TA from AEO_x-TA in serum was investigated. It can be seen in Fig. 2F that AEO_3-TA and AEO_5-TA degraded slowly, and the time of complete degradation was about 30 min. The complete degradation time of AEO_7-TA and AEO_9-TA was about 25 min, while the times of complete degradation of AEO_{12}-TA and AEO_{15}-TA in serum were about 20 and 10 min, respectively. These results indicated that with the growth of the hydrophilic chain of AEO_x-TA, the degradation rate of the ester bond gradually increased. This might be due to the hydrophilic effect, which was conducive to the contact between the ester bond and the esterase active site. Then, the inhibitory effect of TA, a degradation product of AEO_x-TA, on PLA activity was investigated by incubating the degradation product of AEO_x-TA with PLA. As shown in Fig. 2G, the PLA activity of AEO_3-TA, AEO_5-TA, AEO_7-TA, AEO_9-TA, AEO_{12}-TA, AEO_{15}-TA groups were 85%, 72%, 68%, 56%, 38%, and 26%, respectively, and AEO_{15}-TA exhibited the strongest inhibition toward PLA. The results indicated that the inhibition of PLA activity was proportional to the rate of TA released by AEO_x-TA degradation. Then, AEO_x-TA degradation products, PLA, and proMMP9 solution were incubated together to investigate the influence of PLA inhibition on the MMPs. As shown in Fig. 2H, the MMP9 activity was improved when PLA was added, suggesting that PLA can activate the activity of MMP9. However, the MMP9 activities of AEO_3-TA, AEO_5-TA, AEO_7-TA, AEO_9-TA, AEO_{12}-TA, and AEO_{15}-TA groups were 84%, 75%, 66%, 48%, 32%, and 24%, respectively, indicating that TA released by AEO_x-TA degradation could inhibit the activity of PLA and MMPs, which facilitated the accumulation of collagen matrix in the process of tissue fibrosis.

3.6. Investigation of the safety of AEO_x-TA in blood

The safety of *in vivo* application of cationic surfactant is very important. Therefore, the effect of AEO_x-TA on the secondary structure of albumin was investigated by circular dichroism. As shown in Fig. 2I, the absorption peak of circular dichroism at 208 and 222 nm in AEO_3-TA and AEO_5-TA groups significantly changed compared with the control group, indicating that both AEO_3-TA and AEO_5-TA could significantly destroy or alter the secondary structure of albumin. Moreover, AEO_7-TA and AEO_9-TA showed a slight change compared with the control group, indicating that AEO_7-TA and AEO_9-TA could also have a certain damaging effect on the secondary structure of albumin. However, AEO_{15}-TA had the least damaging effect on the secondary structure of albumin, indicating that with the growth of the hydrophilic chain of AEO_x-TA, the destructive effect of surfactant on the secondary structure of protein decreased significantly due to the protective effect of the hydrophilic effect. In addition, the blood safety of AEO_x-TA surfactant was investigated by a hemolysis experiment. As shown in Fig. 2J and K, and Supporting

Information Fig. S5, AEO_x had a hemolytic effect on RBC at concentrations of 1% and 0.1% but did not have an obvious hemolytic effect after dilution to a concentration of 0.01%. This indicated that the hemolytic effect of the surfactant could be significantly reduced after blood dilution. AEO_x-TA surfactant still had a hemolytic effect at a concentration of 0.01%, indicating that cationic surfactant had a strong hemolytic effect on RBC. However, after incubation of AEO_x-TA surfactant with serum for 15 min, it was found that the hemolytic effect decreased to different degrees, among which AEO_{15}-TA had the lowest hemolytic effect. This result indicated that AEO_x-TA could lose the properties of cationic surfactants under the degradation of esterase in blood and significantly reduce the hemolytic effect after blood dilution.

3.7. Evaluation of embolus in mouse tail vein

In order to investigate the blood vessel damage effects of AEO_x-TA/P, photoacoustic imaging was used to detect the damage effects of AEO_x-TA/P on blood transport capacity, with hemoglobin as an indicator. As shown in Fig. 3A and B, fluorescence intensity represents the normal hemoglobin content signal. There was no significant change in fluorescence intensity in the AEO_3-TA/P and AEO_5-TA/P groups, indicating no effect on blood transport capacity. However, there were varying degrees of fluorescence intensity decrease in the POL/P, AEO_7-TA/P, AEO_9-TA/P, AEO_{12}-TA/P, and AEO_{15}-TA/P treatment groups with the lowest fluorescence intensity observed in the AEO_{15}-TA/P group, suggesting that the sclerosant with longer hydrophilic chains significantly decreased blood transport capacity, implying better blood vessel damage effects. Peripheral blood after AEO_x-TA/P treatment was taken for circulating endothelial cells (CECs) count to investigate the shedding of vascular endothelial cells induced by AEO_x-TA damage to blood vessels. The results are shown in Fig. 3C. After AEO_3-TA/P and AEO_5-TA/P treatment, almost no CECs could be detected, indicating that no shedding of vascular endothelial cells occurred. There was obvious shedding of vascular endothelial cells into the blood in the POL/P and AEO_7-TA/P groups. In addition, after AEO_9-TA/P, AEO_{12}-TA/P, or AEO_{15}-TA/P treatment, the most shedding of CECs could be observed in the blood. These results indicated that AEO_x-TA stimulation of vascular injury could induce shedding of endothelial cells, and this effect increased with the increase in the hydrophilicity of AEO_x-TA.

In order to investigate the inhibitory effect of TA, a degradation product of AEO_x-TA, on the process of sclerotherapy, we measured changes in blood PLA levels using ELISA detection. As shown in Fig. 3D, there was no significant change in PLA levels in the AEO_3-TA/P and AEO_5-TA/P groups due to the absence of vascular damage. However, in the POL/P, AEO_7-TA/P, AEO_9-TA/P, AEO_{12}-TA/P, and AEO_{15}-TA/P treatment groups, PLA levels significantly increased, indicating activation of the coagulation-fibrinolysis system after vascular injury. Over-activation of PLA activity can activate the PLA-MMPs system to inhibit tissue fibrosis. We then measured MMP activity in the blood after administration. As shown in Fig. 3E, there was no significant change in MMP activity in the AEO_3-TA/P and AEO_5-TA/P groups due to the absence of vascular damage. In the POL/P administration group, MMP activity increased significantly, as there was no presence of TA to inhibit MMP activity after vascular injury. However, in the AEO_7-TA/P, AEO_9-TA/P, AEO_{12}-TA/P, and AEO_{15}-TA/P treatment groups, MMPs activity decreased gradually, indicating that AEO_x-TA ester bond degradation and the release of TA are beneficial for inhibiting PLA-MMPs activation. Besides, with an increase in the hydrophilic chain, which is favorable for esterase degradation to release TA, MMP activity decreased gradually. We further measured changes in the expression levels of TGF-β1 and M2 macrophages, which play an important role in tissue fibrosis (Fig. 3F−I). In the AEO_3-TA/P and AEO_5-TA/P groups, the expression levels of M2 macrophages and TGF-β1 did not increase significantly. In the POL/P group that did not contain TA, the expression levels increased slightly. However, in the AEO_7-TA/P, AEO_9-TA/P, AEO_{12}-TA/P, and AEO_{15}-TA/P treatment groups, with an increase in the hydrophilic chain, M2 macrophages and TGF-β1 expression levels gradually increased, indicating that AEO_x-TA ester bond degradation to release TA is beneficial for inhibiting PLA-MMPs activity and promoting vascular fibrosis. Additionally, AEO_x-TA with longer hydrophilic chains is more quickly degraded by esterase to release TA and promote the fibrotic process.

The tail vein of Kunming mice was used as an animal vessel model, and the vascular sclerotherapy effect of AEO_x-TA was further investigated *in vivo*. Saline, POL/P foam preparation, and AEO_x-TA/P foam preparation were injected respectively as a negative group, positive group, and experimental group. As shown in Fig. 3J, under the irradiation of 0.5 W LED yellow light, a black mouse tail vein vessel could be clearly seen in the saline, AEO_3-TA/P, and AEO_5-TA/P groups. In the POL/P and AEO_7-TA/P groups, a thin caudal vein could still be seen after treatment, indicating that the vascular sclerotherapy effect of POL or AEO_7-TA was with low efficiency. For AEO_9-TA/P, AEO_{12}-TA/P, and AEO_{15}-TA/P groups, blood vessels were found to have disappeared after treatment on Day 7, indicating that AEO_9-TA, AEO_{12}-TA, and AEO_{15}-TA had vascular sclerotherapy effect. Moreover, adjacent non-administered blood vessels were observed under 0.5 W LED yellow light (Supporting Information Fig. S6). The non-administered veins remained intact in all groups, suggesting that the surfactant sclerosants lose their sclerosing effect on blood vessels when diluted by blood. These results imply that the foam preparation created by surfactant-based sclerosants, a type of mild vascular sclerosant, requires comprehensive contact with the targeted region to effectively manifest their sclerosing efficiency. As the foam transitions into a liquid state during its journey through the bloodstream, it becomes diluted, thus reducing its sclerosing impact on unintended vessels. The vein of the treated mice was sliced and observed by H&E staining, and the results are shown in Fig. 3K. The vein slices of the mice treated with saline, AEO_3-TA/P, and AEO_5-TA/P showed complete hollow vessel outlines without any embolism, while the vein slices of the mice treated with POL/P and AEO_7-TA/P showed that the vessels were not completely embolized, but only narrowed. In the tail vein sections of mice treated with AEO_9-TA/P, AEO_{12}-TA/P, and AEO_{15}-TA/P, blood vessels completely disappeared and were embolized by other tissues. It could be speculated from these results that the vascular sclerotherapy effect of AEO_x-TA gradually increased with the increase of hydrophilicity of AEO_x-TA, and the number of ethylene oxide in hydrophilic fragments of AEO_x-TA used for sclerotherapy should be more than 9 to achieve the purpose of vascular sclerotherapy.

3.8. Evaluation of embolus in rabbit ear marginal vein

Based on the above results, AEO_{15}-TA showed a strong therapeutically cytotoxic effect, inhibition of the PLA system, and better *in vivo* safety. Therefore, AEO_{15}-TA was subsequently

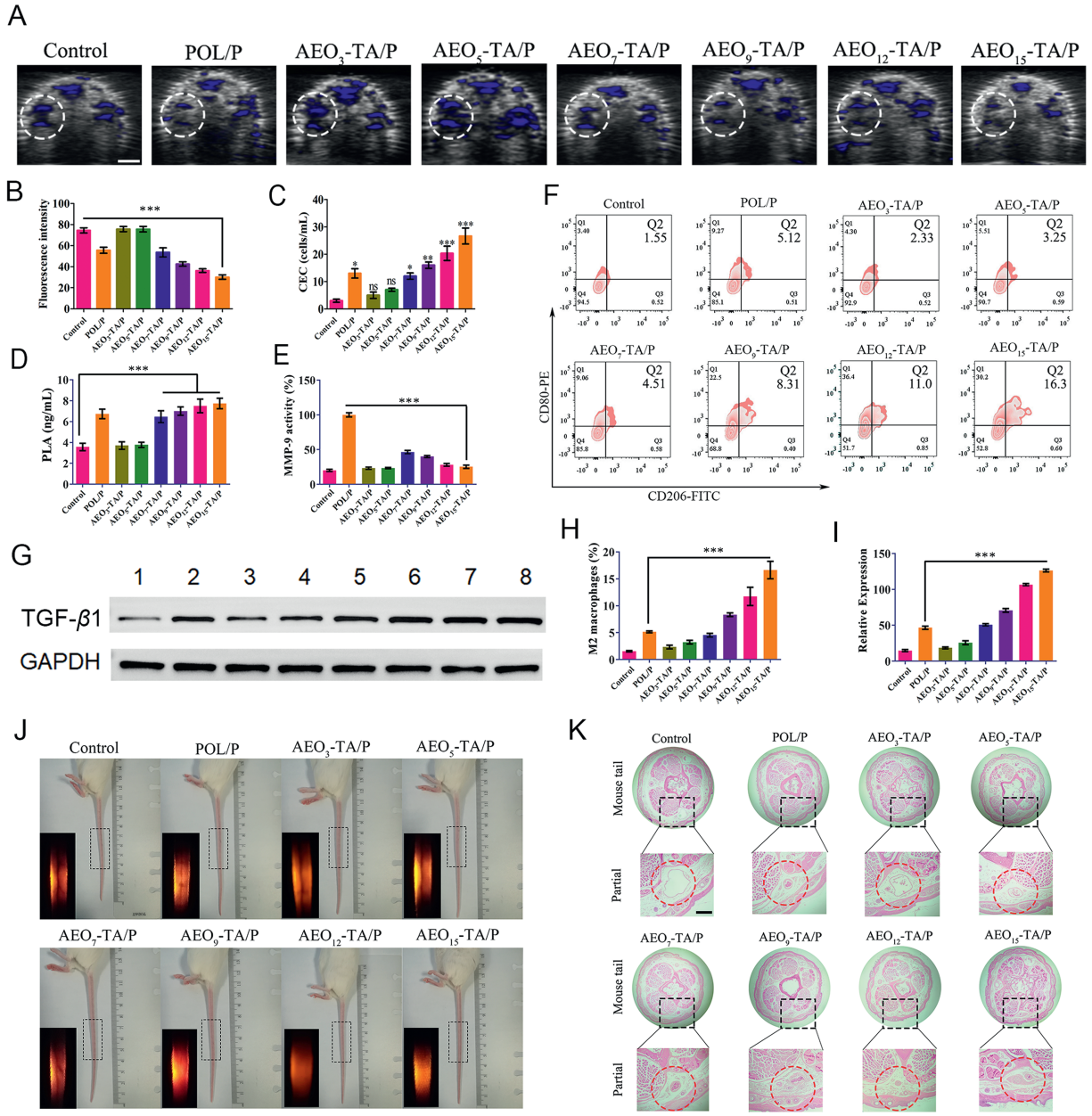

Figure 3 (A) Representative US/PA images of *in vivo* tail tissues. (B) The corresponding PA intensities of drug-administration vein, scale bar = 1 mm. (C) Quantitation of circulating endothelial cells (CECs) in the blood after treatment with saline, POL/P, and AEO_x-TA/P, respectively, at 24 h. (D) PLA level in the blood after treatment with saline, POL/P, and AEO_x-TA/P, respectively, at 24 h. (E) Relative MMP-9 activity in the blood after treatment with saline, POL/P, and AEO_x-TA/P, respectively, at 24 h. (F) and (H) Flow cytometric analyses of M2 macrophages in tail tissues after treatments on Day 3 and populations of $CD80^+CD206^+$ cells. (G) and (I) Protein levels of TGF-β1 in tail tissues after treatments on Day 3 determined by Western blot (1. Control, 2. POL/P, 3. AEO_3-TA/P, 4. AEO_5-TA/P, 5. AEO_7-TA/P, 6. AEO_9-TA/P, 7. AEO_{12}-TA/P, 8. AEO_{15}-TA/P) and cumulative densitometric analyses of the TGF-β1 bands were performed by ImageJ. (J) Photos of the tail veins of Kunming mice after treatment with saline, POL/P, or AEO_x-TA/P on the 7th day. The embedded pictures are the tail vein vessels under 0.5 W yellow LED light. (K) H&E staining of the tail veins of Kunming mice treated with saline, POL/P, and AEO_x-TA/P, respectively, on Day 7, scale bar = 200 μm. Data are presented as mean ± SD (n = 6), $^*P < 0.05$, $^{**}P < 0.01$, $^{***}P < 0.001$; ns, not significant.

selected for further pharmacodynamic evaluation. The rabbit ear marginal vein was used as a model to evaluate sclerotherapy. The rabbits were divided into TA, AEO_{15}/P, AEO_{15}+TA/P, and AEO_{15}-TA/P groups to investigate the sclerosing effect of AEO_x-TA that was based on the dual mechanism of vascular damage and PLA system inhibition. The results are shown in Fig. 4A–C. After TA administration, there was no damage to the ear vein vessels, indicating that TA did not have vascular damage function, nor did it actively cause a coagulation effect, so it was safe for *in vivo* application. After AEO_{15}/P foam treatment, obvious occlusion occurred in ear vein vessels on Day 18. The vessels began to disappear on Day 21, and the disappeared blood vessel was about

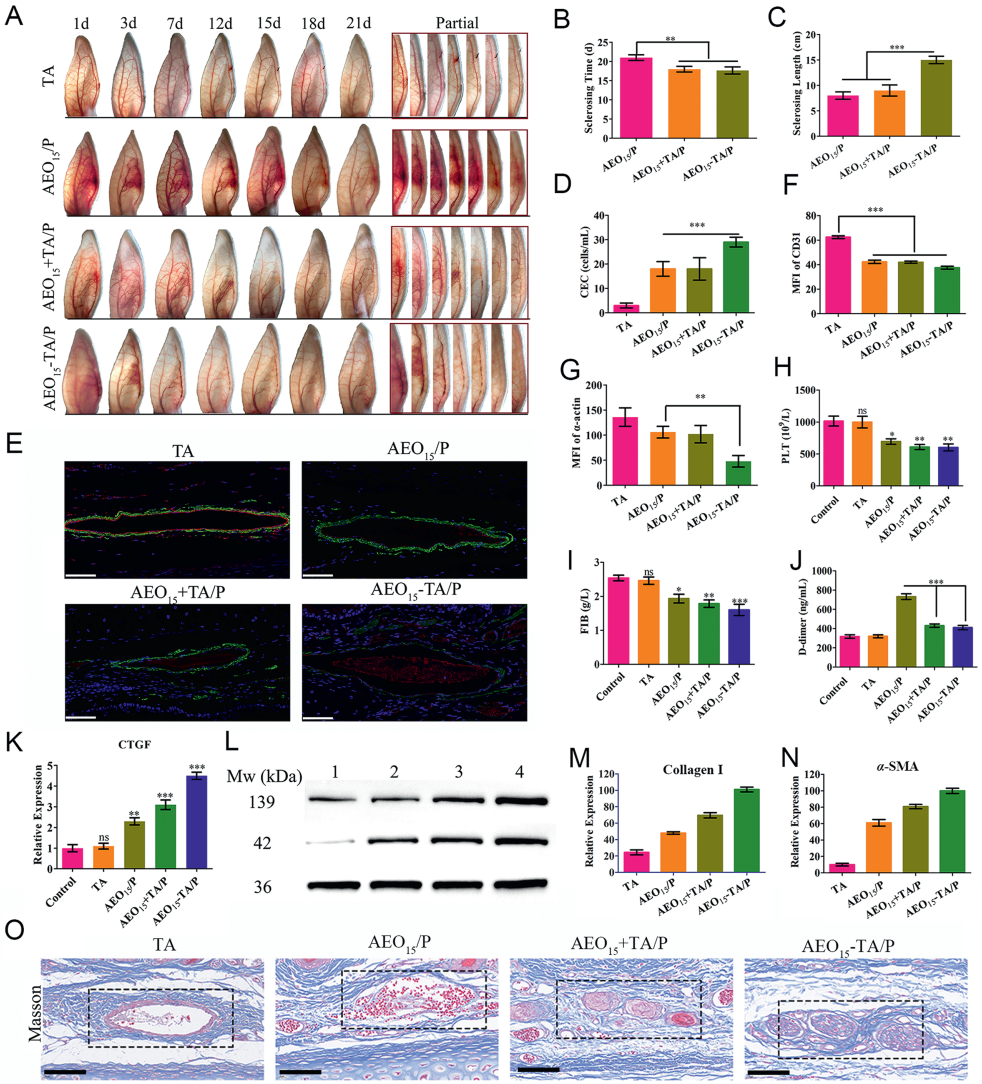

Figure 4 (A) Sclerotherapy study on rabbit ear marginal vein treated with TA, AEO_{15}/P foam preparation, AEO_{15}+TA/P foam preparation, and AEO_{15}-TA/P foam preparation for 21 d, respectively. (B) Sclerosing time of rabbit ear marginal vein after different treatments. (C) Sclerosing length of rabbit ear marginal vein after different treatments on Day 21. (D) Quantitation of circulating endothelial cells (CECs) in the blood after treatments at 24 h. (E), (F,G) Immunofluorescence staining images and mean fluorescent intensity of CD31 and α-actin in rabbit ear marginal vein after different treatments at 24 h, scale bar = 100 μm. (H,I) Quantitation of platelets (PLT) and fibrin (FIB) in the blood after treatments at 24 h. (J) Quantitation of D-dimer in the blood after treatments at 24 h. (K) Relative expression of the signaling factors required by tissue fibrosis (CTGF) in the blood after treatments on Day 7. (L), (M,N) Expression of collagen I (139 kDa) and α-SMA (42 kDa) in rabbit ear, determined by Western blotting. GAPDH was used as an internal reference (1. TA, 2. AEO_{15}/P, 3. AEO_{15}+TA/P, 4. AEO_{15}-TA/P). (O) Masson analyzed the rabbit ear marginal vein after different treatments on Day 12, scale bar = 200 μm. Data are presented as mean ± SD ($n = 6$), $^{*}P < 0.05$, $^{**}P < 0.01$, $^{***}P < 0.001$; ns, not significant.

7 cm. After AEO_{15}+TA/P treatment, obvious occlusion occurred in the blood vessels on Day 12 after injection. The vessels disappeared on Day 18 after injection, and the disappeared blood vessel was about 8 cm. Compared with the AEO_{15}/P treatment group, the disappearance time of blood vessels in the AEO_{15}+TA/P treatment group was shorter, indicating that the dual mechanism of TA by stabilizing thrombus and inhibiting the activity of fibrinolytic system was conducive to sclerotherapy. After treatment with AEO_{15}-TA/P, occlusion occurred in blood vessels on Day 12, blood vessels completely disappeared on Day 18, and the disappeared blood vessel was about 15 cm. Compared with the AEO_{15}/P and AEO_{15}+TA/P groups, the length of disappeared blood vessels in AEO_{15}-TA/P was significantly longer. This indicated that the AEO_{15}-TA, which is a cationic surfactant, showed a stronger vascular destructive effect in the study. Next, through the detection of circulating endothelial cells (CECs), it could be seen that the CECs in the AEO_{15}-TA/P group were significantly more than those in the AEO_{15}/P and AEO_{15}+TA/P groups (Fig. 4D), indicating that the blood vessel damage caused by the cationic surfactant-based AEO_{15}-TA was stronger than that of the AEO_{15}, causing more endothelial cells to fall off into the bloodstream.

3.9. Investigation of AEO_x-TA vascular sclerosis mechanism in vivo using rabbit ear marginal vein as a model

The effect of the sclerosant on the vein wall was investigated by immunofluorescent labeling of vein sections using markers for endothelium (CD31 antibody; in red color) and smooth muscle (α-actin antibody; in green color). The endothelium is the constituent cell of the intima membrane of blood vessels, and smooth muscle is the constituent cell of the media membrane of blood vessels. The results are shown in Fig. 4E−G. After AEO_{15}/P and AEO_{15}+TA/P treatment, the red fluorescence intensity was significantly weakened, while the green fluorescence intensity did not change significantly, indicating that the sclerosing agent could only damage the vascular intima membrane when treated with AEO_{15} alone or a combination of AEO_{15} and TA. The above result suggests that nonionic surfactants had a weak damaging effect on blood vessels. After AEO_{15}-TA/P treatment, the intensity of red fluorescence and green fluorescence of blood vessels were both significantly decreased, which indicated that AEO_{15}-TA/P, a cationic surfactant, could significantly enhance the damaging effect, cause damage to the vascular media membrane. In addition, the contents of fibrin and platelets in blood were measured, and the results are shown in Fig. 4H and I. After treatment with sclerosant, the contents of fibrin and platelets were significantly reduced in AEO_{15}/P, AEO_{15}+TA/P, and AEO_{15}-TA/P groups, indicating the formation of thrombosis after sclerotherapy. Subsequently, the D-dimer was measured, and the contents in TA, AEO_{15}/P, AEO_{15}+TA/P, and AEO_{15}-TA/P groups were 320, 730, 431, and 410 ng/mL, respectively. Compared with the AEO_{15}/P group, the D-dimer contents of the AEO_{15}+TA/P and AEO_{15}-TA/P groups were significantly reduced. These results indicated that TA reduced the degradation effect of PLA on thrombus by inhibiting the activity of PLA, which could prevent ectopic embolism caused by the degradation of thrombus.

The signaling factors required by tissue fibrosis, including CTGF, bFGF, and TGF, were detected to investigate the process of vascular fibrosis. The results are shown in Fig. 4K and Supporting Information Fig. S7. The contents of signaling factors in the sclerotherapy group were higher than those in the control group and TA treatment group. Furthermore, the contents of signaling factors were higher in the AEO_{15}+TA/P and AEO_{15}-TA/P treatment groups than those in the AEO_{15}/P group. These results indicated that TA played an essential role in the expression of fibrosis signaling factors after sclerotherapy. This might be because TA released by AEO_x-TA degradation could inhibit the activity of PLA and MMPs, which influenced the expression of signaling factors for promoting fibrosis. Finally, the vascular tissues after treatment were sliced on Day 12, and Masson staining was used to mark the collagen and fiber tissues. The blue marker was for collagen tissue, and the red marker was for muscle fiber tissue. It could be seen in Fig. 4O that the blood vessels in the TA treatment group were hollow without any damage, indicating that TA had no damage to blood vessels. In addition, it was found that the blood vessels were not completely embolized after AEO_{15}/P treatment, and the blood vessels were filled with less collagen tissue and fiber tissue. However, after AEO_{15}+TA/P treatment and AEO_{15}-TA/P treatment, the blood vessels were obviously embolized and closed, and the center of the blood vessels were filled with collagen tissue and muscle fiber tissue. Subsequently, a Western blot was used to semi-quantitatively determine the expression levels of collagen protein and fibroblast marker protein α-SMA in rabbit ear tissues on Day 12 (Fig. 4L−N). The results indicated that, compared to the AEO_{15}/P and AEO_{15}+TA/P groups, the AEO_{15}-TA/P group exhibited the highest expression level of collagen protein and α-SMA protein, which suggested significant fibroblast proliferation and differentiation. This indicated that TA reduced the degradation of collagen by MMPs and inhibited the PLA-MMPs system, which promoted the proliferation, migration, and differentiation of fibroblasts in vascular tissues, ultimately leading to vascular tissue fibrosis.

In addition, we investigated the *in vivo* safety of AEO_x-TA/P through tissue sections, and the results are shown in Supporting Information Fig. S8. No significant damage was found in the heart, liver, spleen, lung, and kidney after treatment with TA, AEO_{15}/P, AEO_{15}+TA/P, and AEO_{15}-TA/P, respectively. It could be inferred that due to the degradation of AEO_{15}-TA *in vivo*, the damaging effect on non-affected tissue was greatly reduced, indicating that AEO_{15}-TA was adequately safe when applied *in vivo*.

4. Conclusions

Given the dilemma of using sclerotherapy for venous system diseases, we proposed a new vascular sclerotherapy strategy based on vascular damage and PLA system inhibition. Six kinds of AEO_x-TA with different HLB values were constructed by connecting AEO_x compounds with TA. The best sclerosing agent of AEO_x-TA was selected through foam stability tests, cytotoxicity tests, and PLA system inhibition tests. The results showed that AEO_{15}-TA demonstrated a longer hydrophilic structure, the ability to form more uniform stable foams, greater cytotoxicity to venous malformation cells, faster degradation rate in serum, and the ability to significantly inhibit the PLA system. In the rabbit auricular vein vessel model, the vascular damage and PLA system inhibition were further investigated. The results showed that the AEO_{15}-TA, as a cationic surfactant, could cause damage to blood vessels and media membranes due to its stronger cytotoxic effect. Therefore, the effect of vascular sclerosis caused by AEO_{15}-TA was greater than that of AEO_{15}, which is a non-ionic surfactant. In addition, AEO_{15}-TA could release TA to inhibit the PLA-MMPs system, which is conducive to the stability of the thrombus and the release of signaling factors required for tissue fibrosis, collagen deposition, and myofibroblast growth. Therefore, the blood vessels treated with AEO_{15}-TA/P could be embolized in a relatively short time. The dual mechanism of AEO_{15}-TA as a sclerosant lays an important theoretical foundation for the construction of a novel vascular sclerosant.

Acknowledgments

This study was supported by the Shenzhen Natural Science Foundation Project (JCYJ20240813113226035, China), Natural Science Foundation of Top Talent of SZTU (GDRC202305, China), and Basic Scientific Research Funding of Education Department of Liaoning Province (JYTMS20231368, China).

Author contributions

Jizhuang Ma: Software, Methodology, Investigation, Formal analysis, Conceptualization. Keda Zhang: Writing − review & editing, Software, Funding acquisition. Wenhan Li: Validation, Software, Methodology, Formal analysis. Yu Ding: Visualization, Validation, Resources, Project administration. Yongfeng Chen: Writing − review & editing, Data curation. Xiaoyu Huang:

Supervision, Software, Resources, Project administration. Tong Yu: Writing − original draft, Data curation. Di Song: Methodology, Investigation, Formal analysis. Haoran Niu: Software, Resources, Data curation. Huichao Xie: Writing − original draft, Data curation. Tianzhi Yang: Supervision, Methodology, Conceptualization. Xiaoyun Zhao: Visualization, Funding acquisition. Xinggang Yang: Supervision, Project administration, Funding acquisition. Pingtian Ding: Supervision, Funding acquisition, Formal analysis, Conceptualization.

Conflicts of interest

The authors have no conflicts of interest to declare.

Appendix A. Supporting information

Supporting information to this article can be found online at https://doi.org/10.1016/j.apsb.2025.03.032.

References

1. Wetzel-Strong SE, Detter MR, Marchuk DA. The pathobiology of vascular malformations: insights from human and model organism genetics. *J Pathol* 2017;**241**:281−93.
2. Whitehead KJ, Smith MCP, Li DY. Arteriovenous malformations and other vascular malformation syndromes. *Cold Spring Harb Perspect Med* 2013;**3**:a006635.
3. Behravesh S, Yakes W, Gupta N, Naidu S, Chong BW, Khademhosseini A, et al. Venous malformations: clinical diagnosis and treatment. *Cardiovasc Diagn Ther* 2016;**6**:557−69.
4. Horbach SER, Lokhorst MM, Saeed P, de Pontouraude C, Rothova A, van der Horst C. Sclerotherapy for low-flow vascular malformations of the head and neck: a systematic review of sclerosing agents. *Plast Reconstr Surg* 2016;**69**:295−304.
5. Wong M, Parsi K, Myers K, De Maeseneer M, Caprini J, Cavezzi A, et al. Sclerotherapy of lower limb veins: indications, contraindications and treatment strategies to prevent complications—a consensus document of the international union of phlebology-2023. *Phlebology* 2023;**38**:205−58.
6. Prasetyono TOH, Kreshanti P. Efficacy of intra-lesional alcohol injection as alternative and/or complementary treatment of vascular malformations: a systematic review. *Plast Reconstr Surg* 2010;**63**: 1071−9.
7. Zhang L, Chen F, Zheng JT, Wang HW, Qin XJ, Pan WS. Chitosan-based liposomal thermogels for the controlled delivery of pingyangmycin: design, optimization and *in vitro* and *in vivo* studies. *Drug Deliv* 2018;**25**:690−702.
8. Ren JG, Wang HF, Chen G, Zhang W, Jia HZ, Feng J, et al. *In vivo* synergetic effect of in situ sclerotherapy and transient embolotherapy designed for fast-flow vascular malformation treatments with the aid of injectable hydrogel. *J Mater Chem B* 2013;**1**:2601−11.
9. Davis KP, Gaffey MM, Kompelli AR, Richter GT. Cutaneous hyperpigmentation following bleomycin sclerotherapy for vascular malformations. *Pediatr Dermatol* 2022;**39**:103−6.
10. Li XL, Ren XY, Liang JM, Ma WJ, Wang ZH, Yang ZQ. Delivery of sodium morrhuate to hemangioma endothelial cells using immunoliposomes conjugated with anti-VEGFR2/KDR antibody. *Int J Nanomed* 2017;**12**:6963−72.
11. Myers K. A history of injection treatments - II sclerotherapy. *Phlebology* 2019;**34**:303−10.
12. Vandendriessche M, Hobbs JT. The evolution of ultrasound guided foam sclerotherapy. *Acta Chir Belg* 2008;**108**:660−5.
13. Shahat M, Hussein RS, Ahmed AKS. Foam sclerotherapy in pelvic congestion syndrome. *Vasc Endovascular Surg* 2023;**57**:456−62.
14. Nastasa V, Samaras K, Ampatzidis C, Karapantsios TD, Trelles MA, Moreno-Moraga J, et al. Properties of polidocanol foam in view of its use in sclerotherapy. *Int J Pharm* 2015;**478**:588−96.
15. Rial R, Hervas LS, Monux G, Galindo A, Martin A, Hernando M, et al. Polidocanol foam stability in terms of its association with glycerin. *Phlebology* 2014;**29**:304−9.
16. Eckmann DM. Polidocanol for endovenous microfoam sclerosant therapy. *Expert Opin Invest Drugs* 2009;**18**:1919−27.
17. Gao Z, Zhang Y, Li W, Shi C. Effectiveness and safety of polidocanol for the treatment of hemangiomas and vascular malformations: a meta-analysis. *Dermatol Ther* 2018;**31**:e12568.
18. Jacobson BF, Franz RC, Hurly EM, Norman GL, Becker P, Myburgh JA, et al. Mechanism of thrombosis caused by sclerotherapy of esophageal varices using sodium tetradecyl sulphate. *Surg Endosc* 1992;**6**:4−9.
19. Zheng SL, Li ZY, Song J, Wang P, Xu J, Hu WJ, et al. Endothelial METRNL determines circulating METRNL level and maintains endothelial function against atherosclerosis. *Acta Pharm Sin B* 2023; **13**:1568−87.
20. Li HN, Feng Y, Luo Q, Li ZQ, Li X, Gan HT, et al. Stimuli-activatable nanomedicine meets cancer theranostics. *Theranostics* 2023;**13**: 5386−417.
21. Yang Y, Zoulikha M, Xiao QQ, Huang FF, Jiang Q, Li XT, et al. Pulmonary endothelium-targeted nanoassembly of indomethacin and superoxide dismutase relieves lung inflammation. *Acta Pharm Sin B* 2023;**13**:4607−20.
22. Li XT, Zou JH, He ZS, Sun YH, Song XR, He W. The interaction between particles and vascular endothelium in blood flow. *Adv Drug Deliv Rev* 2024;**207**:115216.
23. Zhang WT, Jiang YX, He YL, Boucetta H, Wu J, Chen ZJ, et al. Lipid carriers for mRNA delivery. *Acta Pharm Sin B* 2023;**13**:4105−26.
24. Cullion K, Petishnok LC, Koo H, Harty B, Melero-Martin JM, Kohane DS. Targeting nanoparticles to bioengineered human vascular networks. *Nano Lett* 2021;**21**:6609−16.
25. Jiang YH, Liu JC, Qin JB, Lei JH, Zhang X, Xu ZJ, et al. Light-activated gold nanorods for effective therapy of venous malformation. *Mater Today Bio* 2022;**16**:100401.
26. Sun Y, Gu H, Yang X, Cai R, Shang Y, Hu L, et al. Bleomycin polidocanol foam (BPF) stability—*in vitro* evidence for the effectiveness of a novel sclerosant for venous malformations. *Eur J Vasc Endovasc Surg* 2020;**59**:1011−8.
27. Dong QW, Li X, Dong JX. Branched polyoxyethylene surfactants with different hydrophilic head groups from fatty acid derivatives. *Colloids Surf A Physicochem Eng Asp* 2022;**649**:129419.
28. Xu HJ, Xu YH. Study of the complex system of fatty alcohol polyoxyethylene ether carboxylate and alkyl betaine for heavy oil recovery. *Tenside Surfact Det* 2017;**54**:546−50.
29. Zeng JX, Ge JJ, Zhang GC, Liu HT, Wang DF, Zhao N. Synthesis and evaluation of homogeneous sodium hexadecyl polyoxypropylene ether sulfates. *J Dispersion Sci Technol* 2010;**31**:307−13.
30. Flevaris P, Vaughan D. The role of plasminogen activator inhibitor type-1 in fibrosis. *Semin Thromb Hemost* 2017;**43**:169−77.
31. Lim HI, Hajjar KA. Annexin A2 in fibrinolysis, inflammation and fibrosis. *Int J Mol Sci* 2021;**22**:6836.
32. Farina AR, Cappabianca L, Di Ianni N, Ruggeri P, Ragone M, Merolle S, et al. Alendronate promotes plasmin-mediated MMP-9 inactivation by exposing cryptic plasmin degradation sites within the MMP-9 catalytic domain. *FEBS Lett* 2012;**586**:2366−74.
33. Lemaire R, Burwell T, Sun H, Delaney T, Bakken J, Cheng L, et al. Resolution of skin fibrosis by neutralization of the antifibrinolytic function of plasminogen activator inhibitor 1. *Arthritis Rheumatol* 2016;**68**:473−83.
34. Munakata S, Tashiro Y, Sakamoto K, Okada Y, Heissig B, Hattori K. Inhibition of plasmin protects against experimental colitis by suppressing the matrix metalloproteinase-9-mediated cytokine release from myeloid cells. *Gastroenterology* 2015;**148**:565−78.
35. Sonoki A, Okano Y, Yoshitake Y. Dermal fibroblasts can activate matrix metalloproteinase-1 independent of keratinocytes *via* plasmin in a 3D collagen model. *Exp Dermatol* 2018;**27**:520−5.

36. Saito J, Ishikawa Y, Yokoyama U. Role of tissue-type plasminogen activator in remodeling of the ductus arteriosus. *Circ Rep* 2020;**2**: 211−7.
37. Meng YT, Li ZR, Gong K, An X, Dong JY, Tang PF. Tranexamic acid reduces intraoperative occult blood loss and tourniquet time in obese knee osteoarthritis patients undergoing total knee arthroplasty: a prospective cohort study. *Ther Clin Risk Manag* 2018;**14**:675−83.
38. Yuan XW, Wang JX, Wang QJ, Zhang XL. Synergistic effects of intravenous and intra-articular tranexamic acid on reducing hemoglobin loss in revision total knee arthroplasty: a prospective, randomized, controlled study. *Transfusion* 2018;**58**:982−8.
39. Zheng C, Ma J, Xu JW, Li MY, Wu LM, Wu YA, et al. The optimal dose, efficacy and safety of tranexamic acid and epsilon-aminocaproic acid to reduce bleeding in TKA: a systematic review and bayesian network meta-analysis. *Orthop Surg* 2023;**15**:930−46.
40. Ma JZ, Chen YF, Zhang KD, Yang TZ, Xie HC, Yang XG, et al. Study of vascular sclerosing agent based on the dual mechanism of vascular endothelial cell damage-plasmin system inhibition. *Biochem Biophys Res Commun* 2023;**680**:135−40.
41. del Castillo-Santaella T, Yang Y, Martinez-Gonzalez I, Galvez-Ruiz MJ, Cabrerizo-Vilchez MA, Holgado-Terriza JA, et al. Effect of hyaluronic acid and pluronic-F68 on the surface properties of foam as a delivery system for polidocanol in sclerotherapy. *Pharmaceutics* 2020;**12**:1039.
42. Watkins MR, Oliver RJ. Physiochemical properties and reproducibility of air-based sodium tetradecyl sulphate foam using the Tessari method. *Phlebology* 2017;**32**:390−6.
43. Kochtebane N, Choqueux C, Passefort S, Nataf P, Messika-Zeitoun D, Bartagi A, et al. Plasmin induces apoptosis of aortic valvular myofibroblasts. *J Pathol* 2010;**221**:37−48.